

1 each cell is the average of the Ts across all T field/replicate combinations for the full-mining
2 scenario (300 T fields in total). Not surprisingly, it is clear that the areas of high velocities
3 correspond with the mining zones. The higher velocities and corresponding higher flow rates
4 through the mining zone areas translate to slower velocities in the nonmining zone areas. In
5 most cases, the particles for the mining scenarios stay in the lower velocity zones along the entire
6 pathway to the LWB, which accounts for the higher average travel times. A comparison of the
7 average, maximum, and minimum values for the full-, partial-, and no-mining scenario travel
8 times is presented in Table TFIELD-13.

9 ***TFIELD-9.4.2 Travel Directions***

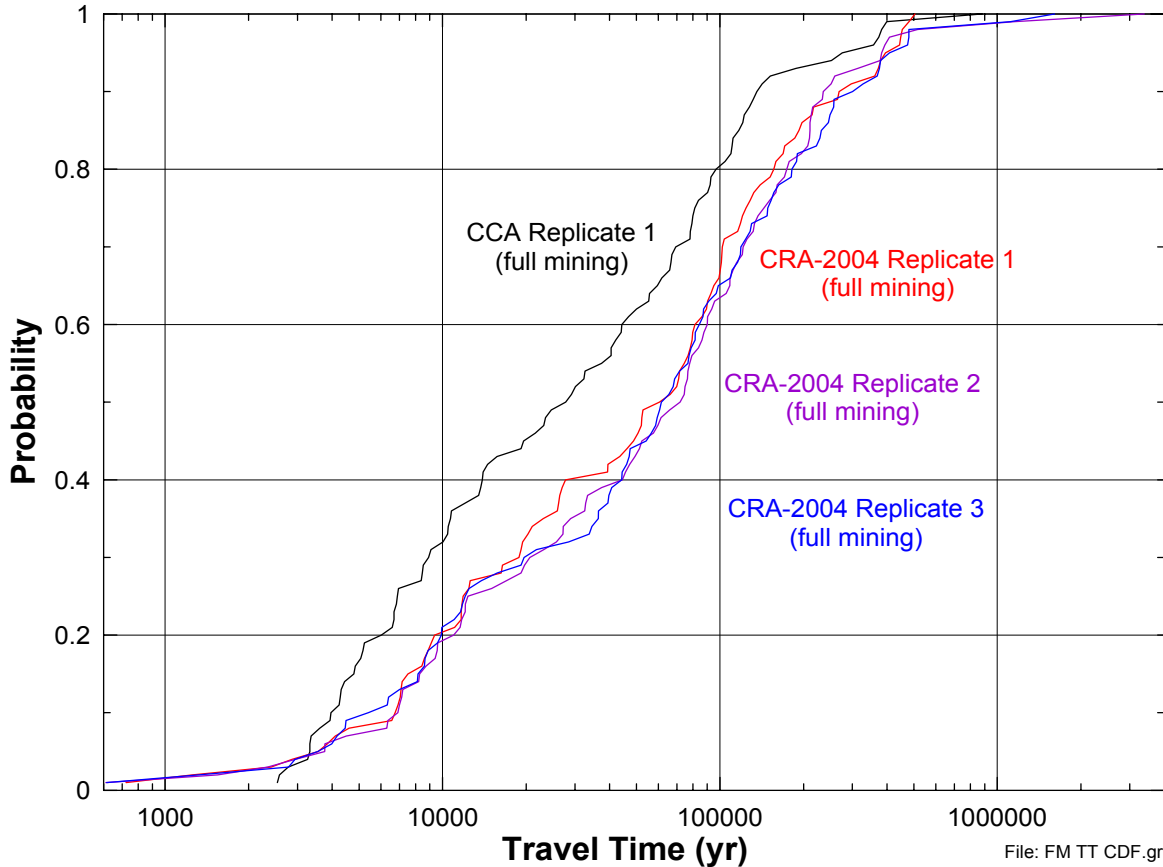
10 The effects of mining also have an impact on the direction of transport, significantly changing
11 where the particles cross the LWB. This is especially true of the full-mining scenario where
12 mining within the LWB creates high head along the eastern boundary of the WIPP resulting in a
13 general flow direction to the westsouthwest. This is in contrast to the partial-mining scenario
14 where the tracking direction is mainly towards the south, similar to the nonmining scenario. The
15 particle-track directions for the partial- and full-mining scenarios are illustrated in Figures
16 TFIELD-73 to TFIELD-78.

17 There is a strong similarity within each replicate for each scenario. Individual tracks can be
18 recognized from one replicate to the next, with some slight variations. This indicates that track
19 directions are determined more by the spatial variation of the calibrated T field than by the
20 random mining factors. As long as there is some (see below) increase in the mining zone Ts
21 over that of the nonmining areas, the tracks for each T field will be similar from one replicate to
22 the next.

23 The partial-mining particle tracks in Figures TFIELD-73 through TFIELD-75 follow paths very
24 similar to the partial-mining particle tracks through the CCA T fields (Ramsey et al. 1996, Figure
25 7.12). The full-mining particle tracks in Figures TFIELD-76 through TFIELD-78 show a more
26 westward component and are generally longer than the full-mining particle tracks through the
27 CCA T fields (Ramsey et al. 1996, Figure 7.13).

28 The insensitivity of the track directions to the random mining factor also carries over to
29 insensitivity of the travel time. Correlation analysis shows correlations between travel time and
30 the random mining factor for the full and partial-mining scenarios as 0.091 and 0.151,
31 respectively. Thus, like the track directions, travel times are not sensitive to the random mining
32 factor but rather to the spatial structure of the calibrated T field.

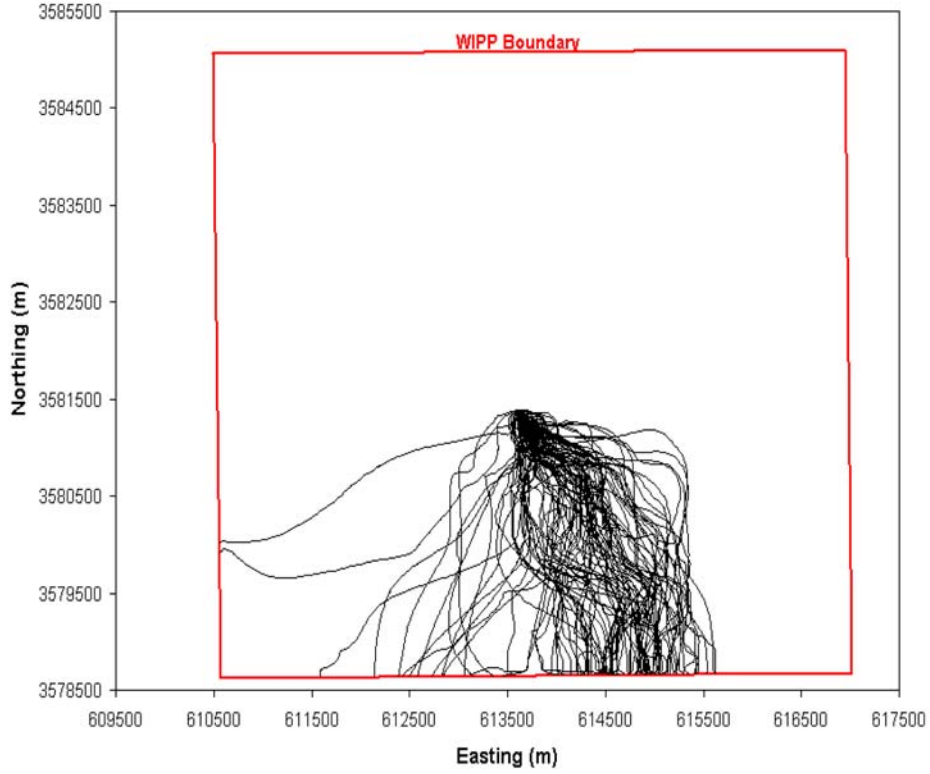
33 This insensitivity to the random mining factor can be explained by recalling that the factor is
34 applied only to zones deemed as probable mining areas. This means that velocity and flow
35 increases are limited to the mining zones, with little change in the nonmining areas (assuming
36 gradients are somewhat constant). Conditions within the nonmining zones are affected most for
37 cases where the mining zone Ts are close to the non-mining zone Ts. However, the mining
38 factor ranges uniformly from 1 to 1,000, meaning 99 percent of the T field/replicate
39 combinations will have multipliers greater than one order of magnitude (for the 300
40 combinations, only two have multipliers that are less than 10). This translates into small changes
41 within the non-mining zones for relatively large changes in the mining zones. To illustrate this,



1
2 **Figure TFIELD-72. CDFs of Full-Mining Travel Times for Three CRA-2004 Replicates**
3 **and One CCA Replicate**

4 **Table TFIELD-13. Travel Time Statistics for the Full- and Partial-Mining Scenarios as**
5 **Compared to the No-Mining Scenario**

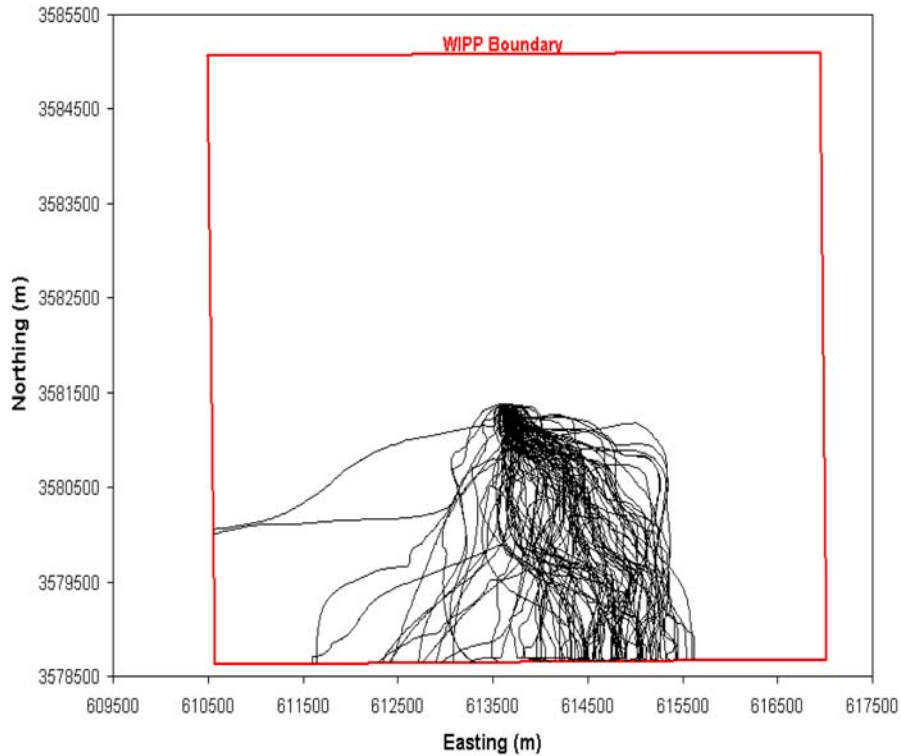
Replicate	Statistic	Full-Mining Travel Time (yr)	Partial-Mining Travel Time (yr)	No-Mining Travel Time (yr)
R1	Median	63,370	47,745	
	Maximum	504,174	494,981	
	Minimum	723	4,684	
R2	Median	73,169	47,651	
	Maximum	3,387,185	531,136	
	Minimum	611	4,654	
R3	Median	63,430	51,622	
	Maximum	1,610,979	506,438	
	Minimum	615	4,603	
Global	Median	66,048	48,290	18,289
	Maximum	3,387,185	531,136	101,205
	Minimum	611	4,603	3,111



1

2

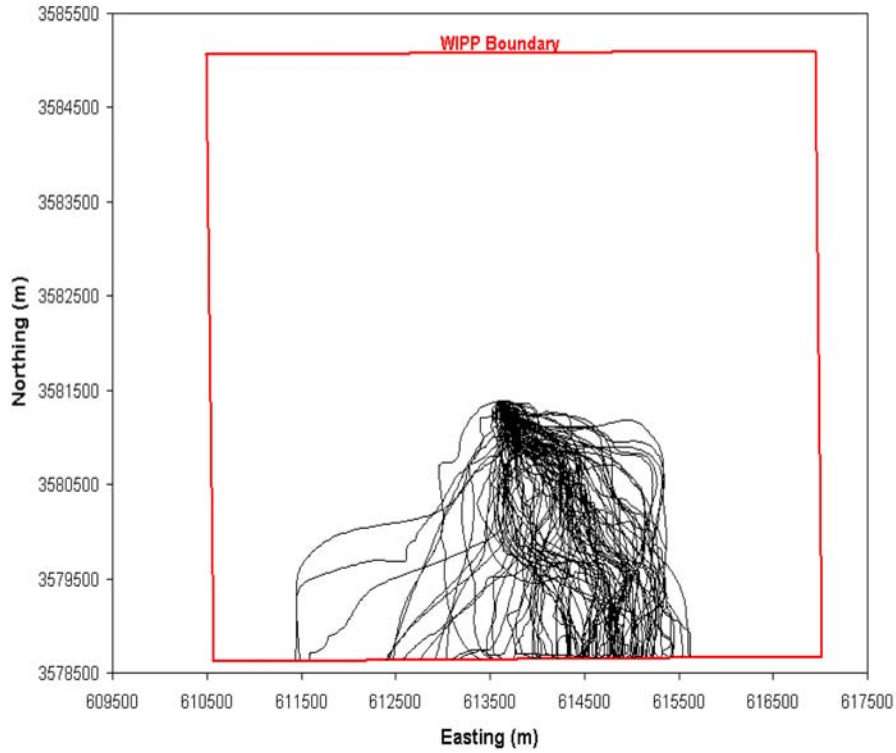
Figure TFIELD-73. Particle Tracks for Replicate 1 for the Partial-Mining Scenario



3

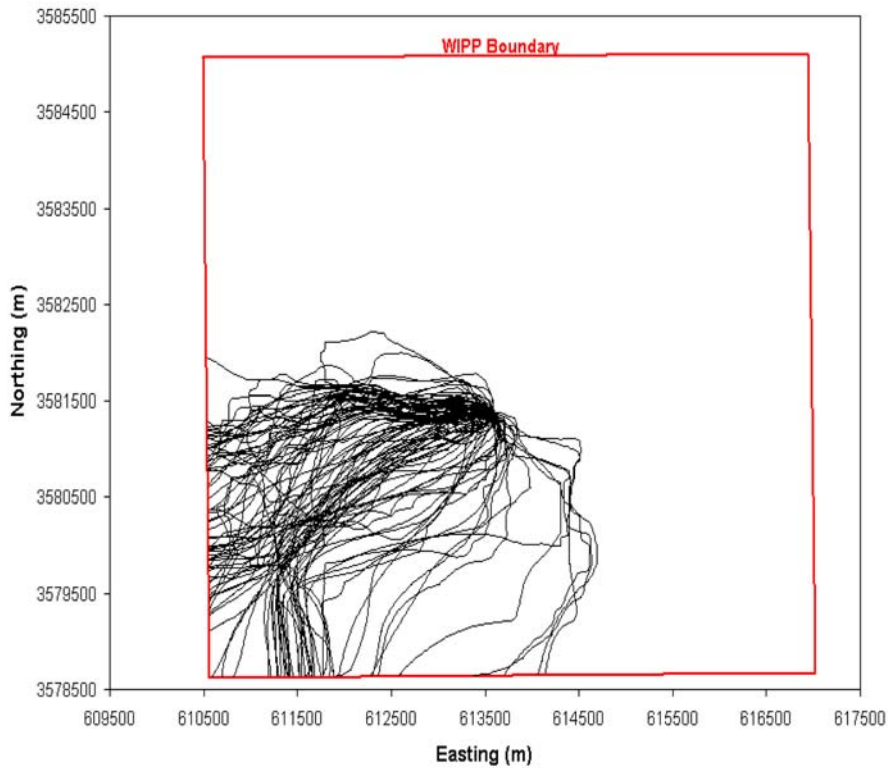
4

Figure TFIELD-74. Particle Tracks for Replicate 2 for the Partial-Mining Scenario



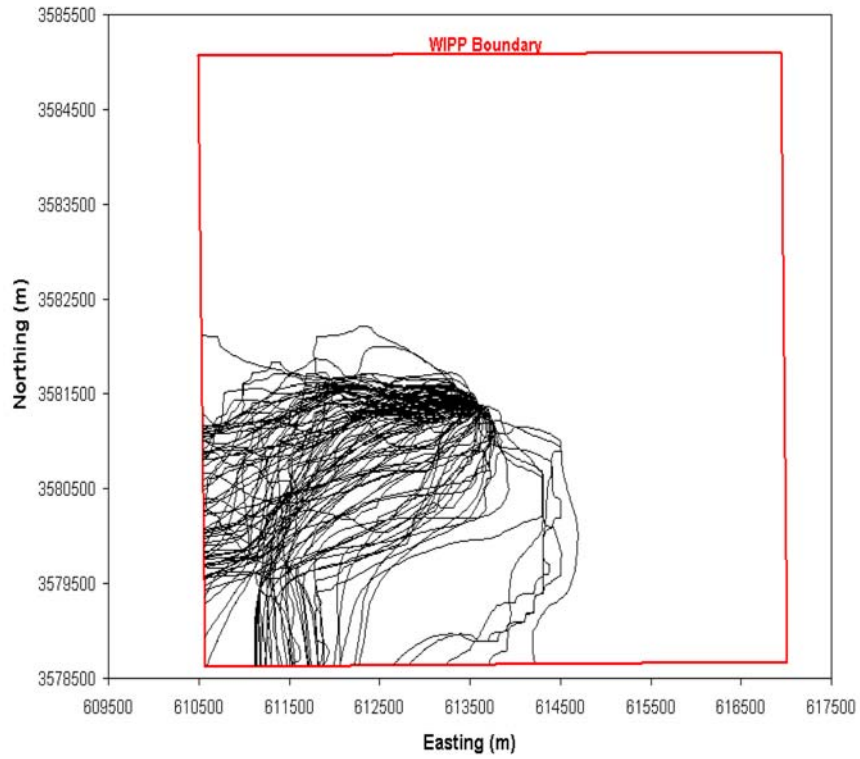
1
2

Figure TFIELD-75. Particle Tracks for Replicate 3 for the Partial-Mining Scenario



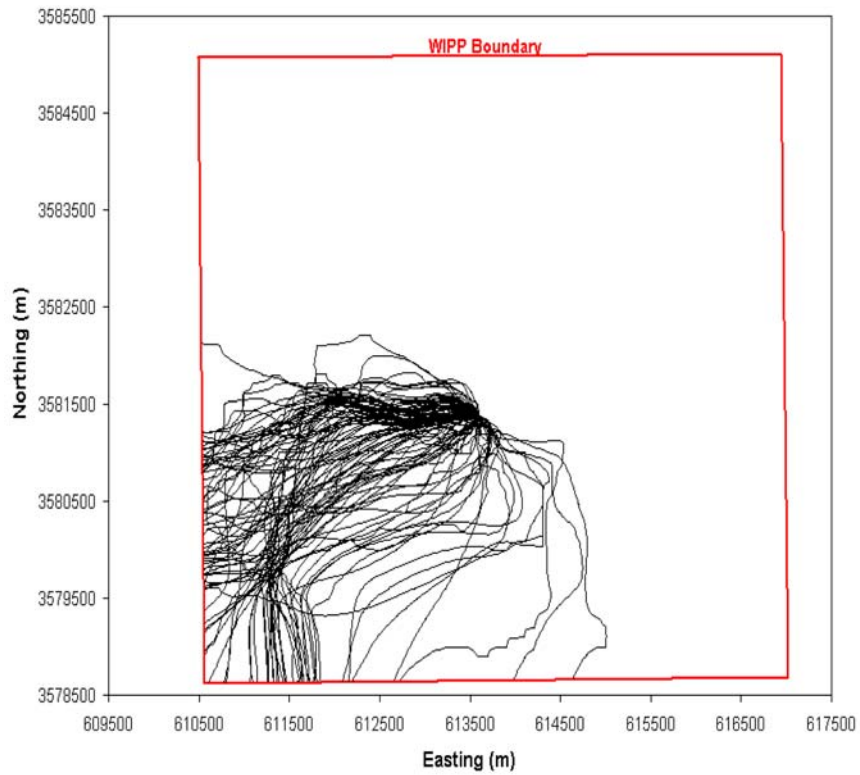
3
4

Figure TFIELD-76. Particle Tracks for Replicate 1 for the Full-Mining Scenario



1
2

Figure TFIELD-77. Particle Tracks for Replicate 2 for the Full-Mining Scenario



3
4

Figure TFIELD-78. Particle Tracks for Replicate 3 for the Full-Mining Scenario

1 Figure TFIELD-79 shows the \log_{10} travel times versus the random mining factor for the full- and
2 partial-mining scenarios across all replicates. The high scatter in both the plots is due to the
3 independence of travel time with regards to the mining factor. This conclusion supports the
4 mining scenario conceptual model and the use of a random mining factor to model changes in T
5 due to mining activities. It also indicates that the controlling parameters are the spatial
6 distribution of the non-mining scenario T field and the delineation of the mining and nonmining
7 zones.

8 ***TFIELD-9.4.3 Extreme Values***

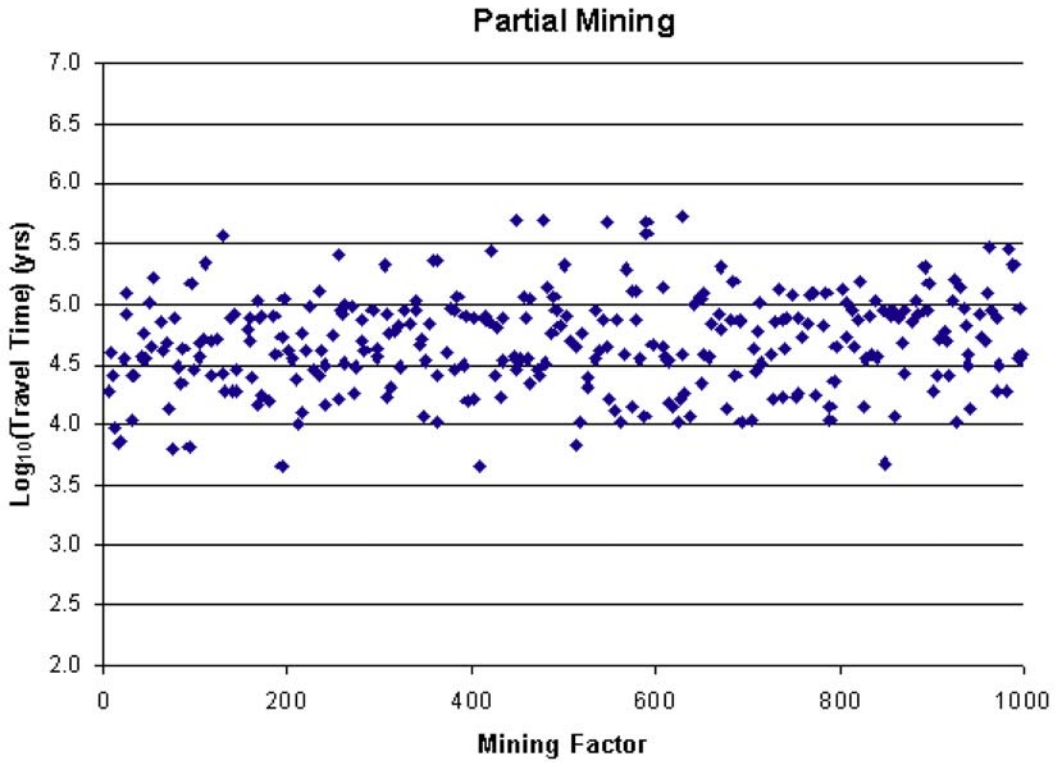
9 Examination of the extreme travel time values and the causes behind those values is useful in
10 quantifying the range of outcomes given the amount of uncertainty incorporated into the models.
11 For the partial-mining scenario, T field d04r01 from Replicate 2 had the longest travel time of
12 531,136 years. In contrast, T field d08r01 from Replicate 3 had the shortest travel time of 4, 603
13 years. The median travel time is best represented by T field d01r04 from Replicate 1 with a
14 travel time of 48, 472 years. Figures TFIELD-80 to TFIELD-82 show the head contours for each
15 of these cases along with the corresponding particle tracks. The particle-tracking directions are
16 all fairly similar.

17 The full-mining cases (Figures TFIELD-83 to TFIELD-85) have similar characteristics to those
18 of the partial-mining cases except that the band of high gradient to the northwest is less
19 pronounced and persistent. For the full-mining scenario, T field d04r01 from Replicate 2 had the
20 longest travel time of 3, 387,185 years. T field d01r07 from Replicate 2 had the shortest travel
21 time of 611 years. The median travel time is best represented by T field d10r09 in Replicate 1
22 (66, 215 years).

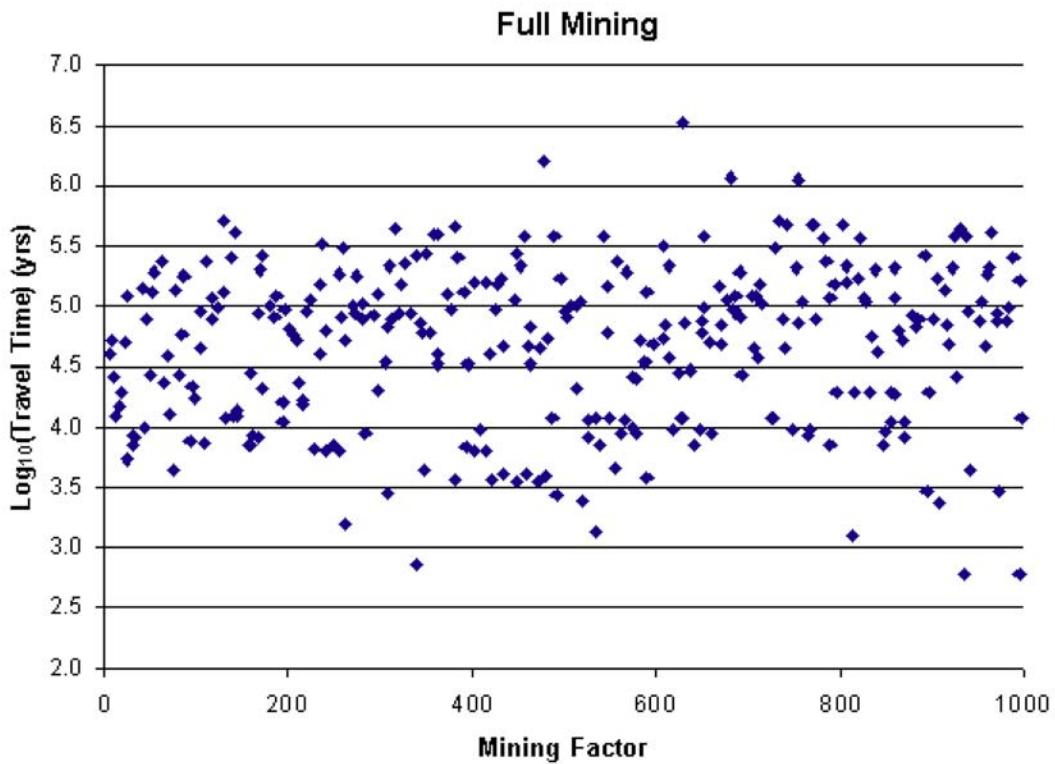
23 Overall, for both the partial- and full-mining scenarios, those T fields that contain higher and
24 more heterogeneous Ts in the nonmining areas produce the fastest travel times. However, the
25 partial-mining scenario shows a smaller range of values due to the lack of the large mining zone
26 in the WIPP area. This smaller range is clearly visible in Figure TFIELD-79. What
27 distinguishes the plots is the head distribution across the regions. For the slow case (Figure
28 TFIELD-80), the head contours to the west of the repository are spread far apart, indicating a low
29 gradient and thus lower groundwater velocities. The fastest case (Figure TFIELD-81) shows a
30 high-gradient band that originates along the no-flow boundary to the northwest and runs down
31 the western side of the WIPP site. This high gradient corresponds to higher groundwater
32 velocities. The median case (Figure TFIELD-82) also shows this high-gradient band, but it is
33 not as extreme as in the fast case. In all cases, the mining-zone areas look very similar, with
34 widely spaced head contours and higher velocities relative to the nonmining zones.

35 ***TFIELD-10.0 SUMMARY***

36 Observed Culebra T has been related to three deterministic factors: the thickness of overburden
37 above the Culebra, the presence or absence of dissolution of the upper Salado, and the presence
38 or absence of halite in units above and below the Culebra. Culebra T is also related to the
39 occurrence of open, interconnected fractures, which cannot be mapped as easily as the other
40 three factors and must be treated stochastically. A linear-regression model for Culebra T has
41 been developed based on these factors that provides an excellent match to the observed data, and

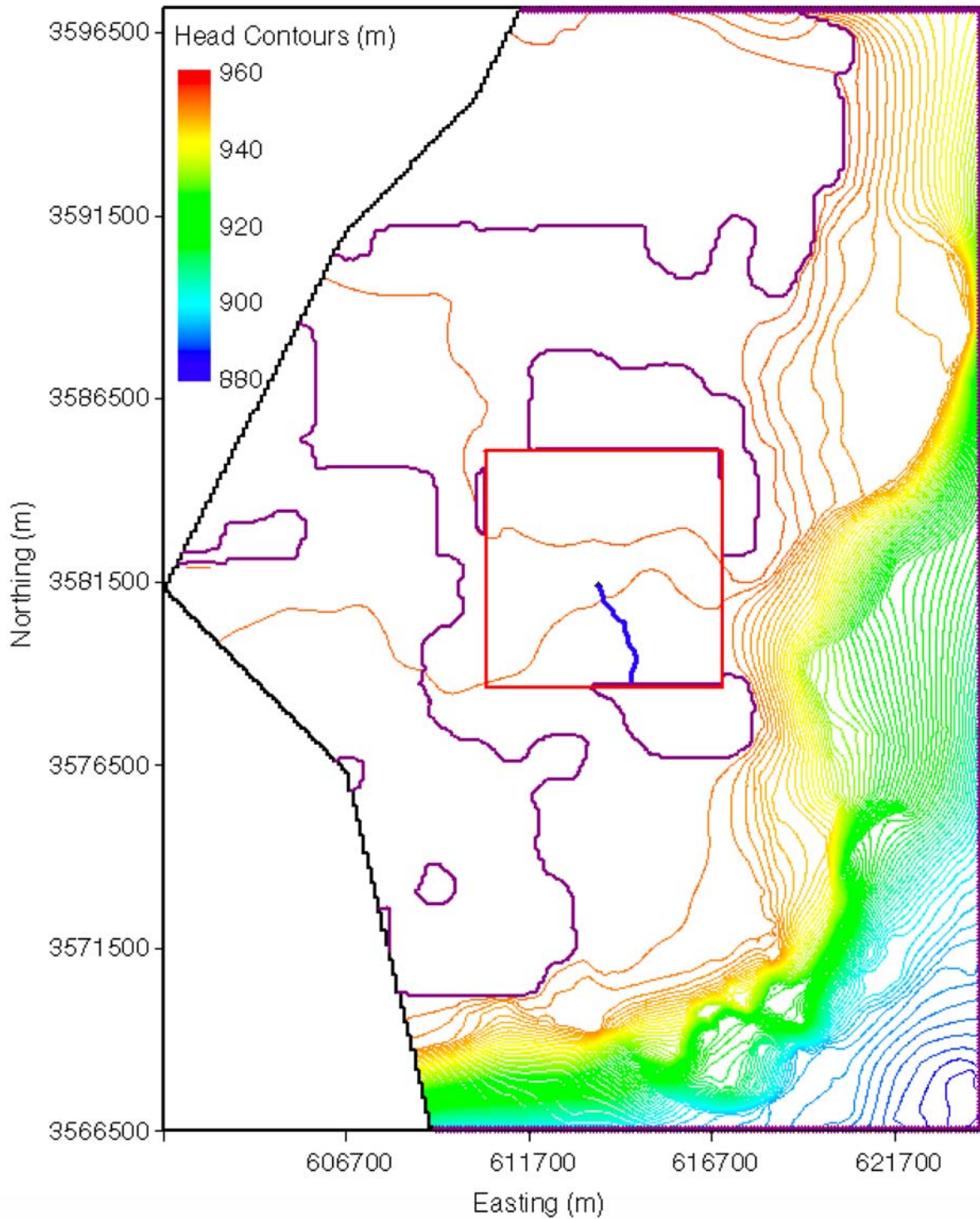


1
2

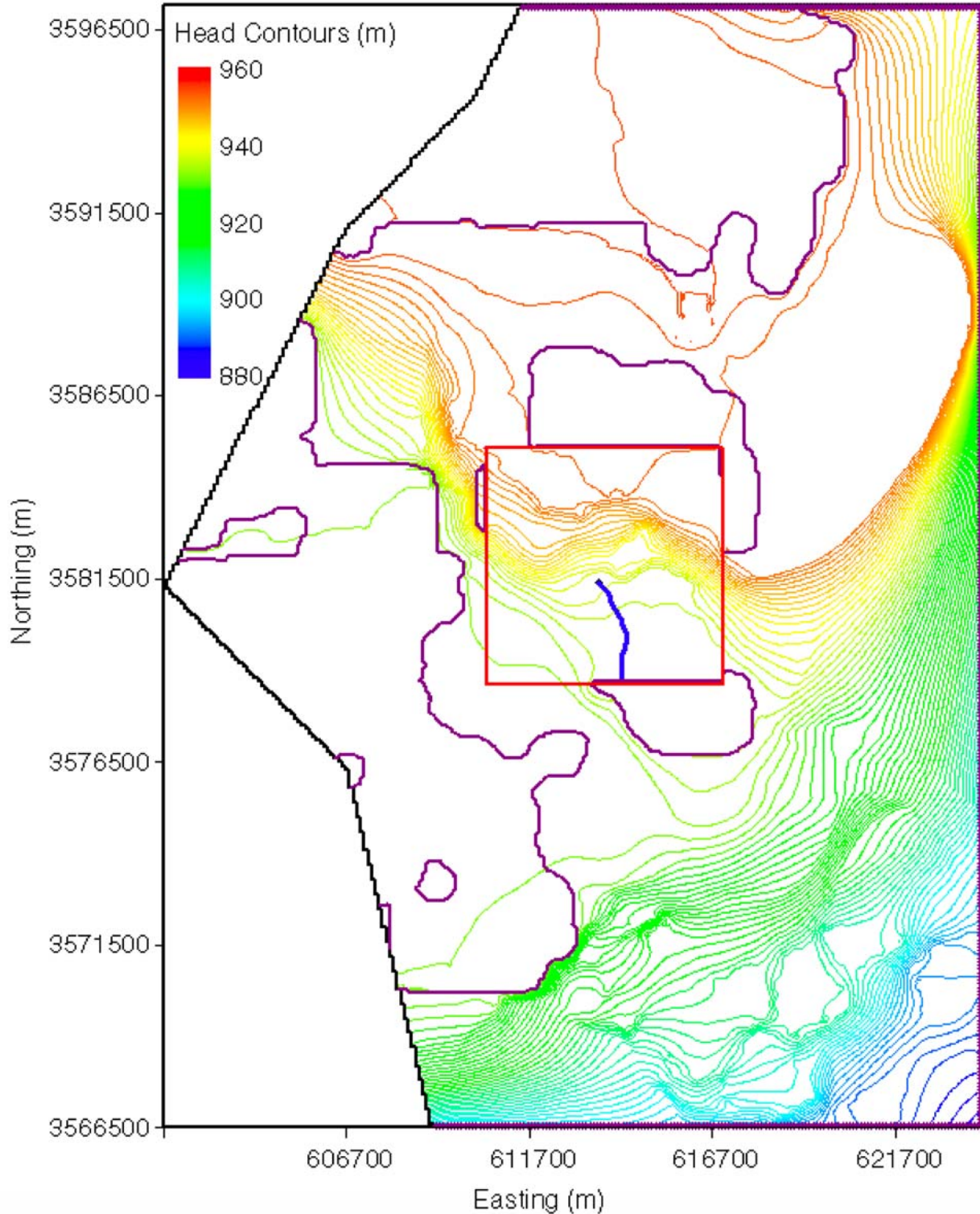


3
4
5

Figure TFIELD-79. Correlation Between the Random Mining Factor and Log₁₀ of Travel Time

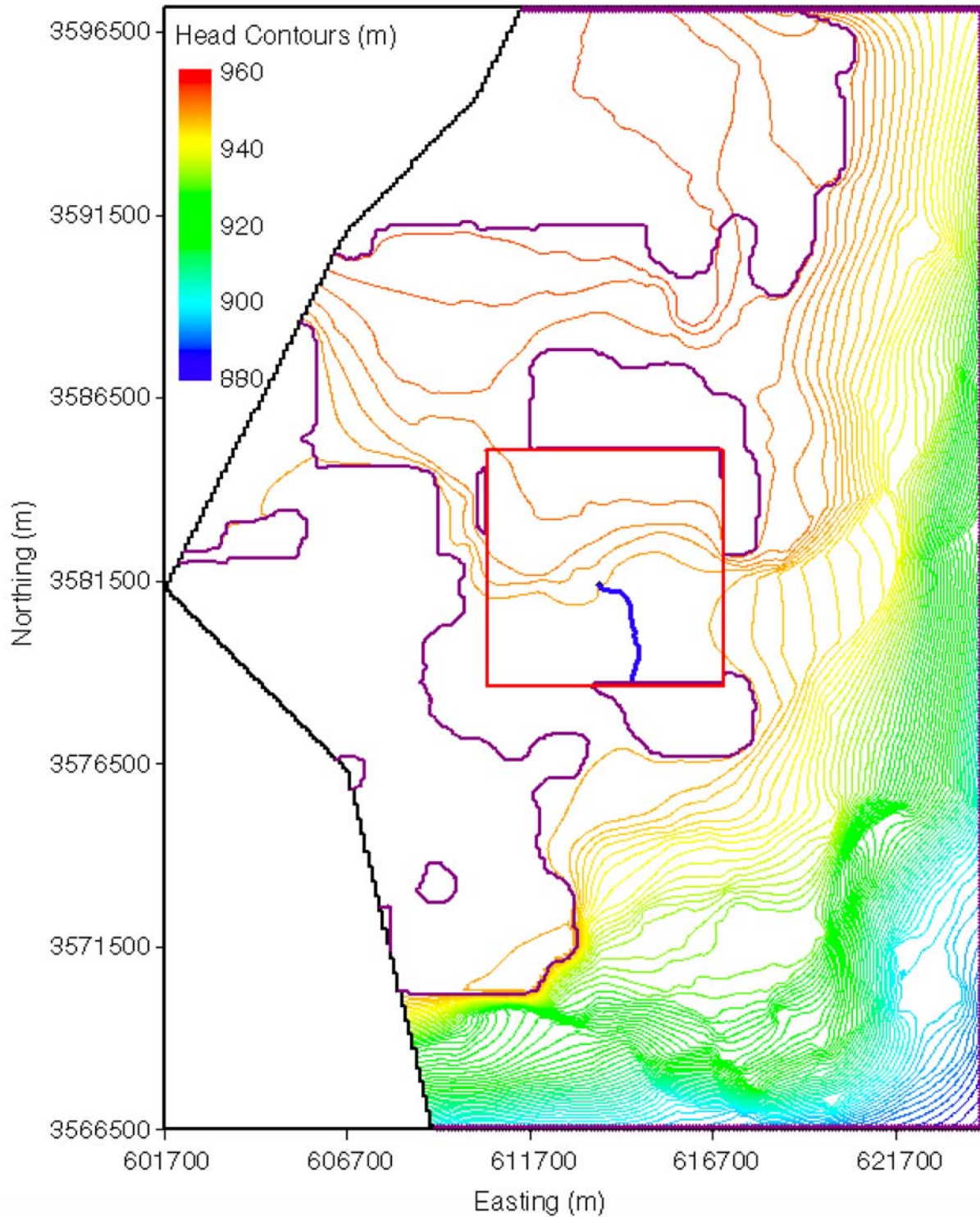


1
2 **Figure TFIELD-80. Head Contours and Particle Track for the Maximum-Travel-Time T**
3 **Field (d04r01-R2) for the Partial-Mining Case. The WIPP LWB is the red box in the**
4 **center of the figure and the particle track is the blue track originating from the**
5 **approximate center of the WIPP.**



1

2 **Figure TFIELD-81. Head Contours and Particle Track for the Minimum-Travel-Time T**
3 **Field (d08r01-R3) for the Partial-Mining Case. The WIPP LWB is the red box in the**
4 **center of the figure and the particle track is the blue track originating from the**
5 **approximate center of the WIPP.**



1
2
3
4
5

Figure TFIELD-82. Head Contours and Particle Track for the Median-Travel-Time T Field (d01r04-R1) for the Partial-Mining Case. The WIPP LWB is the red box in the center of the figure and the particle track is the blue track originating from the approximate center of the WIPP.